Submitted on 21 September 2015.

JOURNAL OF THE ATMOSPHERIC SCIENCES

Statistical state dynamics of jet/wave coexistence in beta-plane turbulence

NAVID C. CONSTANTINOU*

Cyprus Oceanography Center, University of Cyprus, Lefkosia, Cyprus

BRIAN F. FARRELL

Department of Earth and Planetary Sciences, Harvard University, Cambridge, MA, USA

PETROS J. IOANNOU

Department of Physics, National and Kapodistrian University of Athens, Athens, Greece

ABSTRACT

Jets are commonly observed to coexist in the turbulence of planetary atmospheres with planetary scale waves and embedded vortices. These large-scale coherent structures arise and are maintained in the turbulence on time scales long compared to dissipation or advective time scales. The emergence, equilibration at finite amplitude, maintenance and stability of these structures pose fundamental theoretical problems. The emergence of jets and vortices from turbulence is not associated with an instability of the mean flow and their equilibration and stability at finite amplitude does not arise solely from the linear or nonlinear dynamics of these structures in isolation from the turbulence surrounding them. Rather the dynamics of these large-scale structures arises essentially from their cooperative interaction with the small-scale turbulence in which they are embedded. It follows that fundamental theoretical understanding of the dynamics of jets and vortices in turbulence requires adopting the perspective of the statistical state dynamics (SSD) of the entire turbulent state. In this work the S3T implementation of SSD for barotropic beta-plane turbulence is used to develop a theory for the jet/wave coexistence regime.

1. Introduction

A regime in which jets, planetary scale waves and vortices coexist is commonly observed in the turbulence of planetary atmospheres with the banded winds and embedded vortices of Jupiter and the Saturn north polar vortex constituting familiar examples (Vasavada and Showman 2005; Sánchez-Lavega et al. 2014). Planetary scale waves in the jet stream and vortices such as cutoff lows are also commonly observed in the Earth's atmosphere. Conservation of energy and enstrophy in undamped 2D turbulence implies continual transfer of energy to the largest available spatial scales (Fjørtoft 1953). This upscale transfer provides a conceptual basis for expecting the largest scales to become increasingly dominant in the flow as the energy of turbulence forced at smaller scale is continually transferred to the larger scales. However, the observed large-scale structure in planetary atmospheres is dominated not by incoherent large-scale turbulent motion as would be expected to result from the incoherent phase relation of Fourier modes in a turbulent cascade, but rather by coherent zonal jets, vortices and waves of highly specific form. Moreover, the scale of these coherent structures is distinct from the largest scale permitted in the flow. An early attempt to understand the formation of jets in planetary turbulence did not address the structure of the jet beyond attributing the jet scale to arrest of the incoherent upscale energy cascade at the length scale set by the value of the planetary vorticity gradient and a characteristic flow velocity (Rhines 1975). In Rhines's interpretation this is the scale at which the turbulent energy cascade is intercepted by the formation of propagating Rossby waves. This argument has been extended by showing that in addition to energy and enstrophy a third quadratic invariant, zonostrophy, is conserved in dissipationless barotropic β-plane turbulence, which constrains the energy at large scale to be anisotropic, predominantly favoring small zonal wavenumbers (Balk and Yoshikawa 2009). While these results provide a conceptual basis for expecting zonal structures with spatial scale limited by the planetary vorticity gradient to form in beta-plane turbulence, the physical mechanism of formation, the precise morphology of the coherent structures and their stability are not addressed by these general considerations.

*Corresponding author address: Navid Constantinou, University of Athens, Department of Physics, Section of Astrophysics, Astronomy and Mechanics, Building IV, Office 32, Panepistimiopolis, 15784 Zografos, Athens, Greece.

E-mail: navidcon@phys.uoa.gr

Our goal in this work is to develop a general theory that identifies the specific mechanism responsible for the formation of finite amplitude structures in planetary turbulence. A number of mechanisms have been previously advanced to account for jet, wave and vortex formation. One such mechanism for producing jets is vorticity mixing from Rossby wave breaking leading to homogenization of potential vorticity (PV) in localized regions (Baldwin et al. 2007; Dritschel and McIntyre 2008) which results in the case of barotropic beta-plane turbulence in broad retrograde parabolic jets and relatively narrow prograde jets with associated staircase structure in the absolute vorticity. While PV staircases have been obtained in some numerical simulations of strong jets (Scott and Dritschel 2012), vorticity mixing in the case of weak to moderately strong jets is insufficient to produce a prominent staircase structure. Moreover, jets have been shown to form as a bifurcation from homogeneous turbulence in which case the jet is perturbative in amplitude and wave breaking is not involved (Farrell and Ioannou 2003).

Equilibrium statistical mechanics has also been advanced to explain structure emergence e.g. by Miller (1990) and Robert and Sommeria (1991). The principle is that dissipationless turbulence tends to produce configurations that maximize entropy while conserving both energy and enstrophy. These maximum entropy configurations in beta-plane turbulence assume the coarse grained structure of zonal jets or vortices (cf. Bouchet and Venaille (2012)). However, the relevance of these results to the formation, equilibration and maintenance of jets and vortices in strongly forced and dissipated planetary flows remains to be established.

Zonal jets can also arise from modulational instability (Lorenz 1972; Gill 1974; Manfroi and Young 1999; Berloff et al. 2009; Connaughton et al. 2010). This instability produces spectrally non-local transfer to the zonal flow from forced waves and therefore presumes a continual source of waves with the required form. In baroclinic flows, baroclinic instability has been advanced as the source of these waves (Berloff et al. 2009). From the broader perspective of the SSD theory used in this work, modulational instability is a special case of a structural instability predicted by this statistical stability theory (Parker and Krommes 2014; Parker 2014; Bakas et al. 2015). Moreover, while modulational instability addresses formation of jets, it does not predict the formation of non-zonal structures nor does it include the nonlinear mechanisms required to equilibrate the jets at finite amplitude and to predict their structure.

Stochastic structural stability theory (S3T) provides a statistical state dynamics (SSD) based theory for the formation, equilibration and stability of coherent structures in turbulent flows. The underlying mechanism of jet, wave and vortex formation revealed by S3T is the spectrally non-local interaction between the large-scale structure and the small-scale turbulence (Farrell and Ioannou 2003). S3T is a non-equilibrium statistical theory based on a closure comprising dynamics of the coherent structures at large scale together with the consistent second-order fluxes arising from correlations among the components of the field of incoherent eddies. The S3T system is a cumulant expansion of the turbulent dynamics closed at second order (cf. Marston et al. (2008)). In S3T, jets (including meandering jets of planetary scale wave form) initially arise as linear instabilities of infinitesimal perturbations embedded in the field of forced homogeneous turbulence with finite amplitude jets constituting nonlinear equilibria continuing from these instabilities. Analysis of this jet formation instability provides the bifurcation structure of the jet formation process as a function of parameters. S3T predicts both jet and non-zonal structure formation including the formation of finite amplitude nonlinear Rossby waves (zonons) (Bernstein and Farrell 2010; Bakas and Ioannou 2013a, 2014). S3T also predicts the structure of the emergent jets as a function of the relevant dynamical parameters, the structure of the finite amplitude equilibrium jets they continue to, the parameter values at which secondary jet breakdown occurs, the structures these secondary instabilities continue to, and the covariance structure of the turbulence accompanying the jets. The formation of zonal jets in planetary turbulence was studied using S3T by Farrell and Ioannou (2003, 2007, 2008, 2009a,b); Bakas and Ioannou (2011); Srinivasan and Young (2012). A continuous formulation of S3T has facilitated analysis of the mechanism of the S3T instability and construction of analytic expressions for the growth rates of the S3T instability in homogeneous beta-plane turbulence (Srinivasan and Young 2012; Bakas and Ioannou 2013b; Bakas et al. 2015). Recently, the analogy between the dynamics of pattern formation and zonal jet emergence in the context of S3T was studied by Parker and Krommes (2014).

A fundamental attribute of S3T is that eddy–eddy nonlinearity and therefore the nonlinear eddy–eddy cascade is suppressed in the perturbation dynamics. Comparison of the predictions of the theory with sample integrations of the non-linear equations have demonstrated the accuracy of the theory for predicting jet formation and the finite amplitude equilibrated state that result (Srinivasan and Young 2012; Constantinou et al. 2014; Bakas and Ioannou 2014). These results of S3T provide constructive proof that classical cascade theory is not required for jet formation and provide theoretical explanation for observations showing that the turbulent transfers of momentum involved in jet formation and equilibration are non-local in spectral space (Shepherd 1987; Huang and Robinson 1998; Wordsworth et al. 2008; Wordsworth 2009).

S3T predicts that infinitesimal perturbations with jet or planetary wave form organize homogeneous turbulence to produce systematic up-gradient fluxes giving rise to exponential growth and eventually to establishment of finite

amplitude equilibrium straight or meandering jets. The jet formation instability is obtained from the perturbation form of the S3T equations which predict the form and the growth rate of the most unstable eigenmode of the S3T dynamics linearized around the state of homogeneous turbulence.

In this paper we use S3T to further examine the dynamics of the jet/wave coexistence regime in barotropic beta-plane turbulence building on the methods developed by Constantinou (2015).

2. Formulation of the S3T dynamics in barotropic β-plane turbulence

Consider a non-divergent flow $\mathbf{u} = (u, v)$ on a β-plane with coordinates $\mathbf{x} = (x, y)$; in which x is the zonal direction, y the meridional direction. The component of vorticity normal to the plane of motion is $\zeta \equiv \partial_x v - \partial_y u$ and in the presence of dissipation and stochastic excitation the vorticity evolves according to:

$$\partial_t \zeta = -\mathbf{u}\cdot\boldsymbol{\nabla}(\zeta + \beta y) - r\zeta + \nu\Delta\zeta \; + \sqrt{\varepsilon}\xi \; , \qquad (1)$$

with $\Delta \equiv \partial_x^2 + \partial_y^2$ the Laplacian operator. All parameters are non-dimensional. The flow is damped by Rayleigh dissipation with coefficient r and viscous dissipation with coefficient ν. The stochastic excitation ξ is temporally delta-correlated with zero mean, i.e. $\langle \xi(\mathbf{x}, t)\rangle = 0$, and with spatial correlation between between points $\mathbf{x}_a = (x_a, y_a)$ and $\mathbf{x}_b = (x_b, y_b)$ given by the forcing covariance Q:

$$\langle \xi(\mathbf{x}_a, t_1)\xi(\mathbf{x}_b, t_2)\rangle = Q(\mathbf{x}_a - \mathbf{x}_b)\,\delta(t_1 - t_2) \; . \qquad (2)$$

Brackets $\langle \cdot \rangle$ denote an ensemble average over forcing realizations. The stochastic forcing is spatially homogeneous with Fourier representation:

$$Q(\mathbf{x}_a - \mathbf{x}_b) = \int \frac{\mathrm{d}^2\mathbf{k}}{(2\pi)^2}\,\hat{Q}(\mathbf{k})e^{i\mathbf{k}\cdot(\mathbf{x}_a - \mathbf{x}_b)} \; , \qquad (3)$$

with power spectrum $\hat{Q}(\mathbf{k}) \geq 0$, for all values of $\mathbf{k} = (k_x, k_y)$. The energy injected by the stochastic forcing is independent of the state of the system as the stochastic excitation is δ-correlated in time implying that the energy injection rate per unit area by the stochastic forcing can be parametrized by ε.

Consider the statistical state dynamics of (1) in the S3T second-order closure (Farrell and Ioannou 2003). This closure has been shown to provide an accurate and analytically predictive description of the emergence and maintenance of large-scale structure in barotropic (Farrell and Ioannou 2003; Srinivasan and Young 2012; Tobias and Marston 2013; Parker and Krommes 2013, 2014; Bakas and Ioannou 2013a, 2014; Constantinou et al. 2014; Farrell and Ioannou 2015) and baroclinic turbulence (Farrell and Ioannou 2008, 2009b).

The variables of the S3T statistical state dynamics are the first cumulant of the vorticity field $Z(\mathbf{x}, t) \equiv \langle \zeta(\mathbf{x}, t)\rangle$ and the second cumulant $C(\mathbf{x}_a, \mathbf{x}_b, t) \equiv \langle \zeta'(\mathbf{x}_a, t)\zeta'(\mathbf{x}_b, t)\rangle$ of the vorticity deviation from this mean, $\zeta'(\mathbf{x}, t) \equiv \zeta(\mathbf{x}, t) - Z(\mathbf{x}, t)$, which is a function of time, t, and the two spatial variables: $\mathbf{x}_a$ and $\mathbf{x}_b$. In what follows, subscripts in operators acting on C indicate the specific variable the operator is acting on and the point of evaluation. The S3T dynamical system is:

$$\partial_t Z = -\mathbf{U}\cdot\boldsymbol{\nabla}(Z + \beta y) - rZ + \nu\Delta Z + R(C) \; , \qquad (4a)$$

$$\partial_t C = (A_a + A_b)C + \varepsilon\, Q \; , \qquad (4b)$$

where

$$A = -\mathbf{U}\cdot\boldsymbol{\nabla} - \left[\beta\partial_x - (\Delta\mathbf{U})\cdot\boldsymbol{\nabla}\right]\Delta^{-1} - r + \nu\Delta \; , \qquad (5)$$

with Δ^{-1} the inverse Laplacian. A is the operator of the linear perturbation dynamics and it therefore includes the non-normal interaction between the eddies and the instantaneous mean flow $\mathbf{U} = (U, V)$ but neglects explicit representation of the perturbation/perturbation nonlinearity. The ensemble mean equation (4a), which retains the advective nonlinearity, is forced by the ensemble mean Reynolds stress divergence, $R(C)$, that is a linear function of the ensemble mean covariance C,

$$R(C) = -\boldsymbol{\nabla}\cdot\left[\frac{\hat{\mathbf{z}}}{2}\times\left(\boldsymbol{\nabla}_a\Delta_a^{-1} + \boldsymbol{\nabla}_b\Delta_b^{-1}\right)C\right]_{\mathbf{x}_a=\mathbf{x}_b} \; , \qquad (6)$$

with $\hat{\mathbf{z}}$ the unit colorblue vector normal to the (x, y) plane. Notation $\mathbf{x}_a = \mathbf{x}_b$ indicates that the function of two variables $\mathbf{x}_a$, $\mathbf{x}_b$ is to be considered a function of a single variable by setting $\mathbf{x}_a = \mathbf{x}_b = \mathbf{x}$. Because of the non-divergence of the velocity field both the mean and perturbation velocity can be obtained from streamfunctions Ψ and ψ', with the velocities given by $\mathbf{U} = (-\partial_y\Psi, \partial_x\Psi)$ and $\mathbf{u}' = (-\partial_y\psi', \partial_x\psi')$ and the vorticities by $Z = \Delta\Psi$ and $\zeta' = \Delta\psi'$.

Note that the S3T system (4) has been written in general form with the ensemble mean not assumed to be homogeneous in the zonal, x, direction so that non-zonal structures could form, as the blocked states in two-layer baroclinic turbulence (Bernstein and Farrell 2010) or the propagating zonons in barotropic turbulence (Bakas and Ioannou 2013a). We adopt this interpretation because we want to examine the S3T stability of inhomogeneous jet states to non-zonal perturbations.

General formulation of S3T requires expressing the dynamics so as to enforce scale separation between the large and small scale dynamics. This can be implemented by writing corresponding equations to (4) with an explicit scale separation enforced by projection of the dynamics in the mean and perturbation equations on distinct sets of Fourier harmonics. Consider the Fourier expansion of the

vorticity field

$$\zeta = \sum_{k_x}\sum_{k_y} \hat{\zeta}_{\mathbf{k}} e^{i\mathbf{k}\cdot\mathbf{x}} \,, \tag{7}$$

and the projection operator P_K defined as in Frisch (1995):

$$P_K\zeta \equiv \sum_{|k_x|\le K}\sum_{k_y} \hat{\zeta}_{\mathbf{k}} e^{i\mathbf{k}\cdot\mathbf{x}} \,, \tag{8}$$

so that the large-scale flow is identified as $Z \equiv P_K\zeta$ and the small-scale flow as:

$$\zeta' = (I-P_K)\zeta \equiv \sum_{|k_x|>K}\sum_{k_y} \hat{\zeta}_{\mathbf{k}} e^{i\mathbf{k}\cdot\mathbf{x}} \,, \tag{9}$$

with I the identity.

With this interpretation the S3T equations (4) take the form

$$\partial_t Z = P_K\left[-\mathbf{U}\cdot\boldsymbol{\nabla}(Z+\beta y) - rZ + \nu\Delta Z + R(C)\right] \,, \tag{10a}$$

$$\partial_t C = (I-P_{Ka})(I-P_{Kb})\left[(A_a+A_b)C + \varepsilon Q\right] \,. \tag{10b}$$

It can be shown that these equations have the same quadratic conservation laws as the S3T equations (4) and the full nonlinear equations (1). We note that with $K=0$ this projection formulation reduces to the zonal mean/perturbation formulation employed previously to study zonal jet formation using S3T (Farrell and Ioannou 2003).

3. Specification of the parameters used in this work

We choose the large-scale dynamics to include only zonal wavenumbers $k_x = 0,1$ so that the projection P_K has $K=1$. A periodic square channel of size $2\pi\times 2\pi$ is used and the covariance of the homogeneous stochastic forcing is taken to have the anisotropic spectrum:

$$\hat{Q}(\mathbf{k}) = \frac{4\pi k_x e^{-k^2d^2}/N_f}{k_x/|k_x| - \mathrm{erf}(k_x d)} \sum_{k_f\in K_f}\left[\delta(k_x-k_f)+\delta(k_x+k_f)\right] \,, \tag{11}$$

with $k=|\mathbf{k}|$, $d=0.2$, $K_f=\{2,3,\ldots,14\}$ the zonal wavenumbers that are forced and $N_f=13$ the total number of excited zonal wavenumbers. The forcing has been normalized so that each k_f injects equal energy to the flow and the total energy injection rate is unity:

$$\int \frac{\mathrm{d}^2\mathbf{k}}{(2\pi)^2}\frac{\hat{Q}(\mathbf{k})}{2k^2} = 1 \,, \tag{12}$$

and, given the state independence of this temporally uncorrelated forcing, the rate of energy injection by the stochastic forcing in both (1) and (4) is ε.

Simulations are performed using a pseudospectral code with $N_x = N_y = 64$ grid points. Linear damping with $r=0.15$ is included and diffusion coefficient $\nu = 0.01$ is chosen, in order that scales of the order of the grid are damped in unit time. Planetary vorticity gradient $\beta = 10$ was chosen corresponding to a terrestrial length scale of $L = 1200$ km and a time scale of $T = 6$ days.

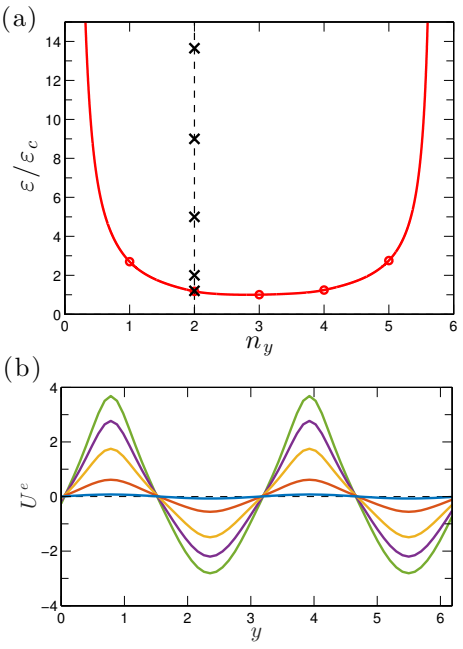

FIG. 1. (a) Normalized turbulent energy input rates, $\varepsilon/\varepsilon_c$, at which the homogeneous state becomes unstable to jet ($n_x=0$) perturbations as a function of the meridional wavenumber n_y. Dots indicate wavenumbers allowed by periodicity in the model used. ε_c is the minimum energy input rate for jet emergence. Here, at $\varepsilon_c = 0.2075$ jets first emerge with y (unallowed) wavenumber $n_y = 2.82$. For $\varepsilon/\varepsilon_c < 1.18$ the homogeneous state is stable to $n_y = 2$ mean flow perturbations and $n_y = 2$ jet equilibria do not exist. (b) The $n_y = 2$ zonal jet S3T equilibrium structure at $\varepsilon/\varepsilon_c = 1.2, 2, 5, 9, 13.65$ (marked with $\times$ in panel (a)). Increasing supercriticality results in increasing jet equilibria mean flow amplitude and deviation of the jet structure from the eigenmode sinusoidal form.

4. S3T jet equilibria

Fixed points of the S3T system correspond to statistical equilibria of the barotropic dynamics. We will study establishment of these statistical equilibria as a function of ε. For all values of ε and all homogeneous stochastic forcings there exist equilibria that are homogeneous (both in x and y) with

$$\mathbf{U}^h = (0,0) \,, \tag{13a}$$

$$C^h(\mathbf{x}_a-\mathbf{x}_b) = \varepsilon\int \frac{\mathrm{d}^2\mathbf{k}}{(2\pi)^2}\frac{\hat{Q}(\mathbf{k})}{2(r+\nu k^2)} e^{i\mathbf{k}\cdot(\mathbf{x}_a-\mathbf{x}_b)} \,, \tag{13b}$$

where $\hat{Q}(\mathbf{k})$ is the power spectrum of the stochastic forcing, defined in (3).

However, these equilibria become unstable when ε exceeds a critical value. For values of ε exceeding this critical value zonal jets arise from a supercritical bifurcation

(Farrell and Ioannou 2007; Srinivasan and Young 2012; Parker and Krommes 2013, 2014; Constantinou et al. 2014). These jets are constrained by the periodic domain of our simulations to take discrete values of meridional wavenumber, n_y. The critical curve in the (ε, n_y) plane separating the region in which only stable homogeneous turbulence equilibria exist from the region in which stable or unstable jet equilibria exist is shown for the chosen parameters in Fig. 1. This marginal curve was calculated using the eigenvalue relation for inhomogeneous perturbations to the homogeneous S3T equilibrium in the presence of diffusive dissipation, in the manner of Srinivasan and Young (2012) and Bakas and Ioannou (2014) with the wavenumber n_y taking continuous values, but with the understanding that only integer values of n_y satisfy the quantization conditions of the channel. S3T instability of the homogeneous state first occurs at $n_y = 2.82$ for $\varepsilon_c = 0.2075$. Jets with $n_y = 3$ emerge at $1.005\varepsilon_c$ and jets with $n_y = 2$ having two maxima at $1.18\varepsilon_c$. Examples of $n_y = 2$ jet equilibria are shown in Fig. 1b. The $n_y = 2$ jet equilibria have mean flows and covariances that are periodic in y with period $\alpha = \pi$ and satisfy the time-independent S3T equations:

$$\left[\frac{1}{2}\left(\partial_{x_a}\Delta_a^{-1} + \partial_{x_b}\Delta_b^{-1}\right) C^e\right]_{\mathbf{x}_a=\mathbf{x}_b} = rU^e - \nu\partial_y^2 U^e \,, \tag{14a}$$

$$\left(A_a^e + A_b^e\right) C^e = -\varepsilon\, Q \,, \tag{14b}$$

with

$$A^e = -U^e\partial_x - \left[\beta - \left(\partial_y^2 U^e\right)\right]\partial_x\Delta^{-1} - r + \nu\Delta \,. \tag{15}$$

A basic property of the jet equilibria, which is shared by all S3T equilibria, is that they are by necessity hydrodynamically stable (cf. Farrell and Ioannou (2015)).[1]

5. S3T stability of the jet equilibria

We are interested in the S3T stability of these $n_y = 2$ jet equilibria to non-zonal perturbations. The stability of jet equilibria to homogeneous in x perturbations has been investigated previously by Farrell and Ioannou (2003, 2007) for periodic domains and by Parker and Krommes (2014); Parker (2014) for infinite domains. A comprehensive methodology for determining the stability of jet equilibria to zonal and non-zonal perturbations was developed by Constantinou (2015). Recalling these results, perturbations $(\delta Z, \delta C)$ about the jet equilibrium state (U^e, C^e), satisfying equations (14), evolve according to:

$$\partial_t\,\delta Z = P_K\left[A^e\,\delta Z + R(\delta C)\right] \,, \tag{16a}$$

$$\partial_t\,\delta C = (I - P_{Ka})(I - P_{Kb})\left[\left(A_a^e + A_b^e\right)\delta C + \left(\delta A_a + \delta A_b\right) C^e\right] \,, \tag{16b}$$

with R defined in (6), A^e defined in (15) and

$$\delta A \equiv -\delta\mathbf{U}\cdot\boldsymbol{\nabla} + (\Delta\delta\mathbf{U})\cdot\boldsymbol{\nabla}\Delta^{-1} \,, \tag{17}$$

where $\delta\mathbf{U} = (-\partial_y\Delta^{-1}\delta Z, \partial_x\Delta^{-1}\delta Z)$ is the perturbation velocity field.

Because of the homogeneity of the jet equilibria in the zonal, x, direction the mean flow eigenfunctions are harmonic functions in x and also because the equilibrium mean flow and covariance are periodic in y with period α, i.e. $U^e(y+\alpha) = U^e(y)$, Bloch's theorem requires that each eigenfunction is a plane wave in y, $e^{iq_y y}$, modulated by a periodic function with period α in y (Cross and Greenside 2009). Therefore, the eigenfunctions take the form:

$$\delta Z = P_K\left[e^{in_x x + iq_y y + \sigma t}\,\delta\tilde{Z}_{n_x,q_y}(y)\right] \,, \tag{18a}$$

$$\delta C = (I - P_{Ka})(I - P_{Kb})\left\{e^{in_x(x_a+x_b)/2 + iq_y(y_a+y_b)/2 + \sigma t}\left[\delta\tilde{C}_{n_x,q_y}(x_a - x_b, y_a, y_b) + \delta\tilde{C}_{n_x,q_y}(x_b - x_a, y_b, y_a)\right]\right\} \,. \tag{18b}$$

with $\delta\tilde{Z}_{n_x,q_y}(y)$ and $\delta\tilde{C}_{n_x,q_y}(x_a - x_b, y_a, y_b)$ periodic functions in y with period α. We have chosen δC to be a symmetric function of $\mathbf{x}$ under the exchange $\mathbf{x}_a \leftrightarrow \mathbf{x}_b$[2].

Only S3T eigenmodes with $n_x \le K$ exist, otherwise the r.h.s. of (18a) is identically zero. The zonal wavenumber, n_x, takes integer values in order to satisfy the periodic boundary conditions in x, and the Bloch wavenumber, q_y, takes integer values in the interval $|q_y| \le \pi/\alpha$, in order to satisfy the periodic boundary conditions in y (Constantinou 2015). The eigenvalue σ determines the S3T stability of the jet as a function of n_x and q_y. The jet is unstable when $\sigma_r \equiv \mathrm{Re}(\sigma) > 0$ and the S3T eigenfunction propagates in x with phase velocity $c_r \equiv -\mathrm{Im}(\sigma)/n_x$ for $n_x \neq 0$. When $n_x = 0$ the eigenfunctions are homogeneous in the zonal, x, direction and correspond to a perturbation zonal jet. When $n_x \neq 0$ the eigenfunctions are inhomogeneous in both x and y and correspond to a wave. These perturbations, when unstable, can form non-zonal large-scale structures that coexist with the mean flow, as those found in Bakas and Ioannou (2014). For jets with meridional periodicity $\alpha = \pi$, q_y can take only the values $q_y = 0, 1$ and because these jets have a Fourier spectrum with power only at the even wavenumbers, a $q_y = 0$ Bloch eigenfunction has power only at even wavenumbers, while a $q_y = 1$ Bloch eigenfunction has power only at odd wavenumbers.

The maximum growth rate, σ_r, of the S3T eigenfunction perturbations to the S3T equilibrium jet with $n_y = 2$ (cf. Fig. 1b) is plotted in Fig. 2a as a function of supercriticality $\varepsilon/\varepsilon_c$ for both perturbations of jet form ($n_x = 0$) and non-zonal form (with $n_x = 1$). Consider first the stability of the S3T jet to jet perturbation, that is to $n_x = 0$

[1] Stability is enforced at the discrete wavenumbers consistent with the finite domain of the problem and not on the continuum of wavenumbers appropriate for an unbounded domain.

[2] The covariance eigenfunction does not need to be symmetric or Hermitian in its matrix representation, but both symmetric and asymmetric parts have the same growth rate. For a discussion of the properties of covariance eigenvalue problems cf. Farrell and Ioannou (2002).

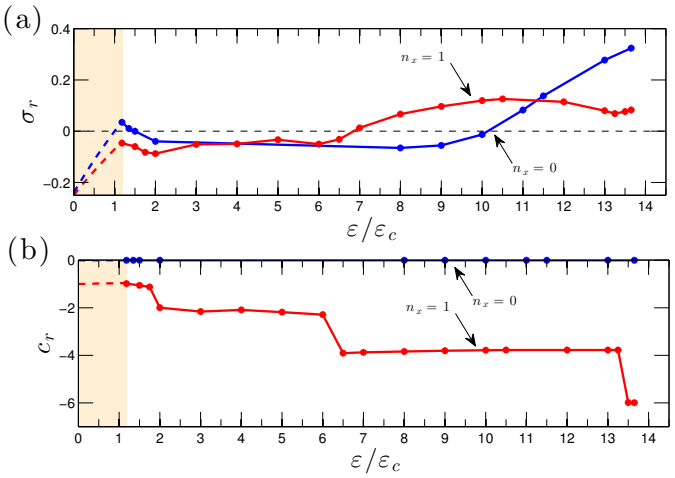

FIG. 2. (a) The maximum S3T growth rates σ_r as a function of $\varepsilon/\varepsilon_c$ for $n_x = 0$ and $n_x = 1$ perturbations to the $n_y = 2$ equilibrium jets. The jet is unstable to jet ($n_x = 0$) perturbations for $1.18 \leq \varepsilon/\varepsilon_c \leq 1.44$ and $\varepsilon/\varepsilon_c \geq 10.14$ and to $n_x = 1$ wave perturbations for $\varepsilon/\varepsilon_c \geq 6.80$. (b) The corresponding phase speeds c_r of the most unstable S3T eigenfunction.

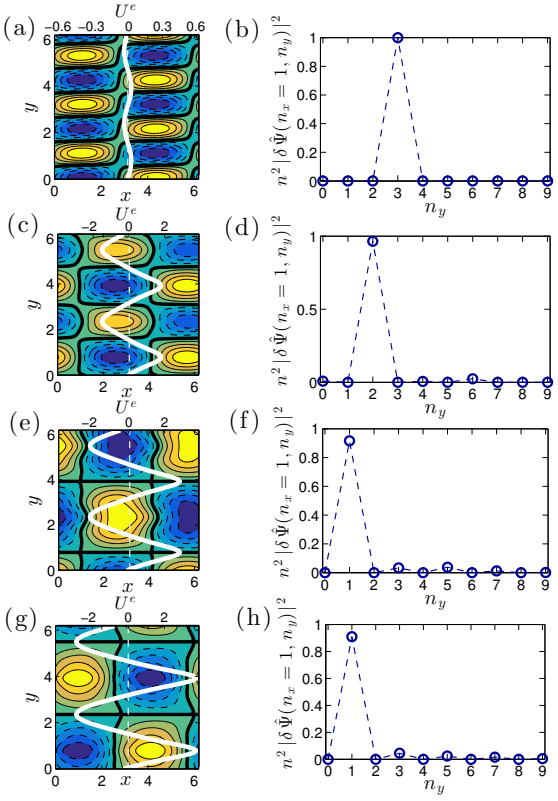

FIG. 3. (a): Contour plot of the streamfunction of the least stable non-zonal $n_x = 1$ S3T mean flow eigenfunction of the $n_y = 2$ jet equilibrium at $\varepsilon/\varepsilon_c = 1.2$ (shown in white) with growth rate $\sigma_r = -0.05$ and phase speed $c_r = -0.98$. The equilibrium jet plotted in solid white. Positive (negative) contours are shown with solid (dashed) lines and the zero contour with thick solid line. (b): The energy power spectrum of the mean flow eigenfunction. This jet equilibrium is unstable to $n_x = 0$ perturbations but stable to $n_x = 1$ perturbations. The least stable $n_x = 1$ eigenfunction is Bloch $q_y = 1$ with power at $n_y = 3$. (c,d): Same for the least stable $n_x = 1$ S3T eigenfunction of the equilibrium at $\varepsilon/\varepsilon_c = 5$. The jet is stable both to $n_x = 0$ and $n_x = 1$ perturbations and the least stable $n_x = 1$ eigenfunction ($\sigma_r = -0.03$, $c_r = -2.18$) is Bloch $q_y = 0$ with power at $n_y = 2$. (e,f): Same plots for the maximally growing $n_x = 1$ S3T eigenfunction of the jet at $\varepsilon/\varepsilon_c = 9$. The jet is stable to $n_x = 0$ perturbations but unstable to $n_x = 1$ perturbations and the most unstable $n_x = 1$ eigenfunction ($\sigma_r = 0.1$, $c_r = -3.81$) is Bloch $q_y = 1$ with power at $n_y = 1$. (g,h): Same plots for the maximally growing $n_x = 1$ S3T eigenfunction of a strong equilibrium jet at $\varepsilon/\varepsilon_c = 13.65$. The most unstable $n_x = 1$ eigenfunction ($\sigma_r = 0.08$, $c_r = -5.99$) is Bloch $q_y = 1$ with power at $n_y = 1$. In this case, $n_x = 0$ perturbations are more unstable with $\sigma_r = 0.32$.

eigenfunctions. Recall that the jets with $n_y = 2$ emerge at $\varepsilon/\varepsilon_c = 1.18$, and for $\varepsilon/\varepsilon_c < 1.18$ (shaded region in Fig. 2a) there are no $n_y = 2$ equilibria. The dashed line shows the smallest decay/fastest growth rate of perturbations to the homogeneous equilibrium state that exists prior to jet formation. The most unstable eigenfunctions of the homogeneous equilibria at these ε are jets with wavenumber $n_y = 3$ (not shown, cf. Fig. 1a). The small amplitude equilibrated $n_y = 2$ jets that form when ε marginally exceeds the critical $\varepsilon/\varepsilon_c = 1.18$ are unstable to jet formation at wavenumber $n_y = 3$ with jet eigenfunction similar to the maximally growing $n_y = 3$ eigenfunction of the homogeneous equilibrium. This S3T instability of the small amplitude $n_y = 2$ jet equilibria to $n_y = 3$ jet eigenfunctions, which is induced by the $n_y = 3$ instability of the nearby homogeneous equilibrium, was identified by Parker and Krommes (2014) as the universal Eckhaus instability of the equilibria that form near a supercritical bifurcation. The Eckhaus unstable S3T $n_y = 2$ jets are attracted to the S3T $n_y = 3$ stable jet equilibrium over the small interval $1.18 < \varepsilon/\varepsilon_c < 1.44$. At higher supercriticalities in the interval $1.44 < \varepsilon/\varepsilon_c < 10.14$ the $n_y = 2$ jets become stable[3] to $n_x = 0$ eigenfunctions. The jets eventually become unstable to $n_x = 0$ eigenfunctions for $\varepsilon/\varepsilon_c > 10.14$. The most unstable $n_x = 0$ eigenfunction at $\varepsilon/\varepsilon_c = 11$ is a Bloch $q_y = 1$ eigenfunction, dominated by a $n_y = 1$ jet that will make the jets of the $n_y = 2$ equilibrium merge to form a $n_y = 1$ jet equilibrium (cf. Farrell and Ioannou (2007)).

The maximum growth rate of the jet equilibria to $n_x = 1$ non-zonal eigenfunctions is also shown in Fig. 2a. Unlike the jet eigenfunctions, which are stationary with respect to the mean flow, these eigenfunctions propagate in the retrograde direction with respect to the jet; the phase velocity of the eigenfunction with maximum real part eigevalue is plotted as a function of $\varepsilon/\varepsilon_c$ in Fig. 2b. Eigenfunctions with $n_x = 1$ are stable for jets with $\varepsilon/\varepsilon_c \leq 6.80$ and when they become unstable the jet is still stable to jet ($n_x = 0$) perturbations. The structure of the least damped/fastest growing eigenfunctions at various $\varepsilon/\varepsilon_c$ are shown in Fig. 3. In Fig. 3a,b is shown the least stable eigenfunction of the weak jet at $\varepsilon/\varepsilon_c = 1.2$. The eigenfunction is Bloch $q_y = 1$ with almost all power at $n_y = 3$. The phase velocity of this eigenfunction is $c_r = -0.98$ which is slightly slower than the Rossby phase speed -1 (i.e., $-\beta/k^2$, with $\beta = 10$, $k_x = 1$, $k_y = 3$). In Fig. 3c,d is shown the least stable $n_x = 1$ mode for the jet at $\varepsilon/\varepsilon_c = 5$ which is Bloch $q_y = 0$ with almost all power at $n_y = 2$ and phase speed $c_r = -2.18$, which corresponds to a slightly modified Rossby phase speed with effective PV gradient of $\beta_{\text{eff}} = 10.9$ instead of the $\beta = 10$ of the uniform flow. In Fig. 3e-h are shown the maximally unstable $n_x = 1$ eigenfunctions for the jets at $\varepsilon/\varepsilon_c = 9$ and $\varepsilon/\varepsilon_c = 13.65$. Both are Bloch $q_y = 1$ with almost all power at $n_y = 1$. At $\varepsilon/\varepsilon_c = 9$ the mode is trapped in the retrograde jet, a region of reduced PV gradient, and the structure of this mode as well as its phase speed corresponds, as will see in the next section, to that of an external Rossby wave confined in this equilibrium flow. At $\varepsilon/\varepsilon_c = 13.65$ the eigenfunction is trapped in the prograde jet, a region of high PV gradient, and the structure of this mode as well as its phase speed corresponds to that of an external Rossby wave in this equilibrium flow.

6. The mechanism destabilizing S3T jets to $n_x = 1$ non-zonal perturbations

We now examine the stability properties of the $n_y = 2$ equilibrium jet maintained in S3T at $\varepsilon/\varepsilon_c = 9$. At $\varepsilon/\varepsilon_c = 9$ the jet is stable to $n_x = 0$ jet S3T perturbations but unstable to $n_x = 1$ non-zonal perturbations with maximally growing eigenfunction growth rate $\sigma_r = 0.097$ and phase speed $c_r = -3.806$, which is retrograde at speed 1.61 with respect to the minimum velocity of the jet.

Because the jet U^e is an S3T equilibrium the operator A^e is necessarily stable to perturbation at zonal wavenumbers that are retained in the perturbation dynamics, i.e. $k_x \in K_f$. The maximum growth rate of operator A^e as a function of k_x for the jet $\varepsilon/\varepsilon_c = 9$ is shown in Fig. 4a, with the integer valued wavenumbers that are included in the S3T dynamics and are responsible for the stabilization of the jet indicated with a circle in this figure. This equilibrium jet, despite its robust hydrodynamic stability at all wavenumbers, in both the mean and perturbation equations, and especially its hydrodynamic stability to $n_x = 1$ perturbations, is nevertheless S3T unstable at $n_x = 1$.

Although it is not formed as a result of a traditional hydrodynamic instability, this S3T instability is very close in structure to the least stable eigenfunction of A^e at $n_x = 1$, as it can be seen in Fig. 4c,d. The spectrum of A^e at $n_x = 1$ is shown in Fig. 4b. The eigenfunctions associated with this spectrum consist of viscous shear modes with phase speeds within the flow and a discrete number of external Rossby waves with phase speeds retrograde with respect to the minimum velocity of the flow (cf. Kasahara (1980)). In this case there are exactly 5 external Rossby waves with phase speeds $c_r = -3.70, -9.80, -5.92, -2.33, -2.37$ all decaying with $k_x c_i = -0.15, -0.16, -0.17, -0.18, -0.24$ respectively. We identify the S3T $n_x = 1$ unstable eigenfunction, shown in Fig. 4d, which has phase speed $c_r = -3.806$ with S3T destabilization of the least stable of the external Rossby waves, shown in Fig. 4c, that has phase speed $c_r = -3.70$. This instability arises by Reynolds stress feedback that exploits the least damped mode of A^e, which is already extracting some energy from the

[3] The periodic boundary conditions always allow the existence of a jet eigenfunction with zero growth and with structure that of the y derivative of the equilibrium jet and covariance. This eigenfunction leads to a translation of the equilibrium jet and its associated covariance in the y direction. This existence of this neutral eigenfunction can be a verified by taking the y derivative of (14). We do not include this obvious neutral eigenfunction in the stability analysis.

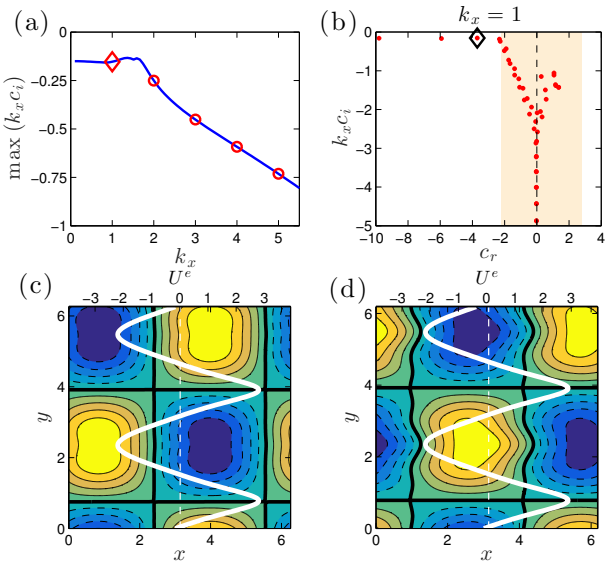

FIG. 4. (a) The hydrodynamic stability of U^e at $\varepsilon/\varepsilon_c = 9$. Shown are the maximal modal growth rates, $k_x c_i$, of operator A^e as a function of k_x. Circles indicate the growth rate at the k_x retained in the perturbation dynamics; diamond indicates the growth rate at $k_x = 1$. The equilibrium jet is hydrodynamically stable but S3T unstable to $n_x = 1$ perturbation. (b) The growth rates, $k_x c_i$, and phase speeds, c_r, of the least damped eigenvalues of A^e for $k_x = 1$ perturbations. The shaded area indicates the region $\min(U^e) \le c_r \le \max(U^e)$. The jet U^e is shown in white in both panels (c) and (d). The streamfunction of the maximally growing S3T $n_x = 1$ eigenfunction is shown in (d). This S3T eigenfunction arises from destabilization of the least damped mode of A^e with $k_x c_i = -0.15$ and $c_r = -3.70$, indicated with the diamond in (b) and shown in (c). The $n_x = 1$ S3T instability with $\sigma_r = 0.097$ and phase speed $c_r = -3.805$ is supported in this case solely by energy transfer from the mean flow U^e (at the rate $\sigma_{10} = 0.3$) against the negative energy transfer from the small scale perturbation field (at the rate $\sigma_{1>} = -0.016$) and dissipation (at the rate $\sigma_{1D} = -0.188$), with the growth rate of the S3T instability being $\sigma_r = \sigma_{10} + \sigma_{1>} + \sigma_{1D}$.

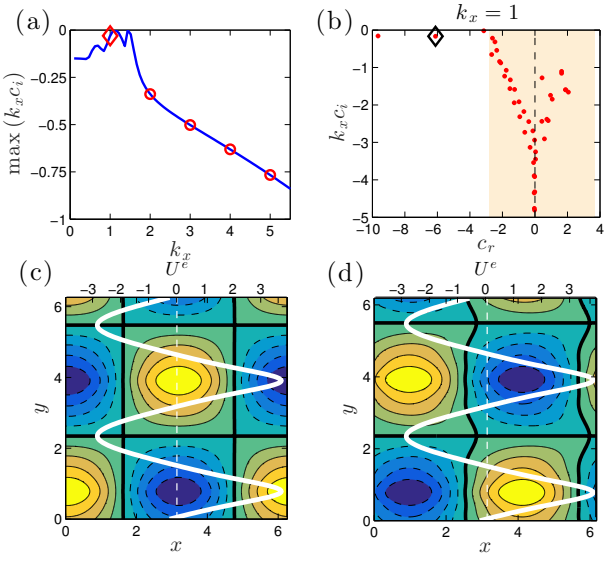

FIG. 5. (a) The hydrodynamic stability of U^e at $\varepsilon/\varepsilon_c = 13.65$. Shown are the maximal modal growth rates, $k_x c_i$, of operator A^e as a function of k_x. Circles indicate the growth rate at the k_x retained in the perturbation dynamics; diamond indicates the growth rate at $k_x = 1$. The equilibrium jet is hydrodynamically stable but S3T unstable to both $n_x = 0$ and $n_x = 1$ perturbations. (b) The growth rates, $k_x c_i$, and phase speeds, c_r, of the least damped eigenvalues of A^e for $k_x = 1$ perturbations. The shaded area indicates the region $\min(U^e) \le c_r \le \max(U^e)$. The jet U^e is shown in white in both panels (c) and (d). The streamfunction of the maximally growing S3T $n_x = 1$ eigenfunction is shown in (d). This S3T eigenfunction arises from destabilization of the second least damped mode of A^e with $k_x c_i = -0.165$ and $c_r = -6.12$, indicated with a diamond in (b) and shown in (c). The $n_x = 1$ S3T instability with $\sigma_r = 0.083$ and $c_r = -5.99$ is supported in this case by both energy transfer from the mean flow U^e (at the rate $\sigma_{10} = 0.16$) and energy transfer from the small scale perturbation field (at the rate $\sigma_{1>} = 0.115$). The dissipation rate is $\sigma_{1D} = -0.192$.

jet through the hydrodynamic instability process, thereby making it S3T unstable. This feedback process transforms a mode of the system that while extracting energy from the mean nevertheless was decaying at a rate 0.15 into an unstable mode growing at rate 0.1. Consistently, note in Fig. 4d that the streamfunction of the S3T eigenfunction is tilting against the shear indicative of its gaining energy from the mean flow.

We quantify the energetics of the S3T instability in order to examine the instability mechanism in more detail. The contribution to the growth rate of this $n_x = 1$ eigenfunction from interaction with the mean equilibrium jet is

$$\sigma_{10} = \frac{1}{2}\frac{(A_{\rm inv}(U^e)\,\delta Z, \delta Z) + (\delta Z, A_{\rm inv}(U^e)\delta Z)}{(\delta Z, \delta Z)}\,, \qquad (19)$$

where $(f,g) \equiv -(2\pi)^{-2}\int \mathrm{d}^2\mathbf{x}\,\frac{1}{2} f\Delta^{-1} g$ is the inner product in energy metric and

$$A_{\rm inv}(U) = -U\partial_x - \left[\beta - (\partial_y^2 U)\right]\partial_x\Delta^{-1}\,, \qquad (20)$$

is the inviscid part of (5) with $V = 0$. The contribution to the growth rate of the $n_x = 1$ eigenfunction from Reynolds stress mediated interaction with the small scales is

$$\sigma_{1>} = \frac{1}{2}\frac{(\delta Z, R(\delta C)) + (R(\delta C), \delta Z)}{(\delta Z, \delta Z)}\,. \qquad (21)$$

The net growth rate of perturbation the $n_x = 1$ eigenfunction is then $\sigma_r = \sigma_{10} + \sigma_{1>} + \sigma_{1\rm D}$, with

$$\sigma_{1\rm D} = \frac{1}{2}\frac{(A_{\rm D}\,\delta Z, \delta Z) + (\delta Z, A_{\rm D}\delta Z)}{(\delta Z, \delta Z)}\,, \qquad (22)$$

the loss to dissipation, with

$$A_{\rm D} = -r + \nu\Delta\,, \qquad (23)$$

the dissipation part of operator (5).

For the S3T unstable eigenfunction shown in Fig. 4d, the growth rate $\sigma_r = 0.097$ arises solely from interaction with the mean flow, which contributes $\sigma_{10} = 0.3$, while the Reynolds stress divergence is downgradient and contributes negatively $\sigma_{1>} = -0.016$ with dissipation accounting for the remainder $\sigma_{1\rm D} = -0.19$. Interestingly, this S3T unstable mode is solely supported in its energetics by induced non-normal interaction with the mean jet and loses energy to the Reynolds stress feedback which is responsible for the instability. This is a remarkable mechanism: it suggests that S3T can transform damped waves into exponentially growing waves by changing the wave structure so as to tap the energy of the mean jet even while the Reynolds stresses that maintain the structure of the wave transfer energy from the wave to the incoherent eddy field. This mechanism of destabilization differs fundamentally from the more familiar S3T instabilities in which jets and waves arise from homogeneous turbulence with energy source exclusively from the incoherent eddy field.

This same mechanism is responsible for the S3T destabilization of the $n_x = 1$ perturbation to the jet equilibrium at $\varepsilon/\varepsilon_c = 13.65$. However, at $\varepsilon/\varepsilon_c = 13.65$ the jet is unstable to both $n_x = 0$ (with maximum growth rate $\sigma_r = 0.32$) and to $n_x = 1$ non-zonal perturbations (with maximum growth rate $\sigma_r = 0.08$ and phase speed $c_r = -5.99$, which is retrograde by 3.18 with respect to the minimum velocity of the jet). This equilibrium flow is also hydrodynamically stable at all the zonal wavenumbers allowed by periodicity (cf. Fig. 5a). This $n_x = 1$ unstable eigenfunction (cf. Fig. 5d) arises from destabilization of the second least damped mode, which is the damped external Rossby mode indicated in Fig. 5b and shown in Fig. 5c. The energetics of the instability indicate that the growth of this $n_x = 1$ structure arises almost equally from energy transferred from the mean equilibrium jet to the $n_x = 1$ perturbation ($\sigma_{10} = 0.16$) and energy transferred by the Reynolds stress divergence of the small scales ($\sigma_{1>} = 0.115$).

7. Equilibration of the S3T instabilities of the equilibrium jet

We examine the equilibration of the $n_x = 1$ S3T instability at $\varepsilon/\varepsilon_c = 9$ and the equilibration of the S3T instabilities at $\varepsilon/\varepsilon_c = 13.65$, which has both $n_x = 0$ and $n_x = 1$ unstable eigenfunctions.

Consider the energetics of these large scales consisting of the $k_x = 0$ and $k_x = 1$ Fourier components. We denote the $k_x = 0$ and $k_x = 1$ components of vorticity of (10a) as Z^0 and Z^1 and the corresponding components of the Reynolds stress divergence as R^0, R^1 and with $Z^e \equiv -\partial_y U^e$ the vorticity of the equilibrium zonal jet. We will study the energetics of the equilibration of the S3T instabilities after removing the constant flux to the large scales from the small scales that maintains the equilibrium flow U^e. For that reason the Reynolds stress divergence of the deviation of the instantaneous covariance from C^e will be considered in the equilibration process.

Consider first the energetics of the $k_x = 1$ component of the large-scale flow. The first contribution to the energy growth of this component is the energy transferred from the $k_x = 0$ component of the flow. This proceeds at the rate:

$$\mathscr{E}_{10} = \left(A_{\rm inv}(U^0)Z^1, Z^1\right) + \left(Z^1, A_{\rm inv}(U^0)Z^1\right)\,, \qquad (24)$$

with $A_{\rm inv}$ defined in (20) and U^0 the total $k_x = 0$ component of the zonal velocity. The second energy source is energy transferred to $k_x = 1$ from the small scales (i.e. those with $|k_x| > K$), which proceeds at the rate:

$$\mathscr{E}_{1>} = \left(Z^1, R^1\right) + \left(R^1, Z^1\right)\,, \qquad (25)$$

with $R^1 \equiv R^1(C - C^e)$ the Reynolds stress divergence produced by covariance $C - C^e$. Finally energy is dissipated

at the rate:

$$\mathscr{E}_{1\mathrm{D}} = \left(A_{\mathrm{D}}Z^1, Z^1\right) + \left(Z^1, A_{\mathrm{D}}Z^1\right) \ , \tag{26}$$

with A_{D} defined in (23).

The energy flows to the $k_x = 0$ component consist first of $\mathscr{E}_{01}$, the energy transfer rate to this component from the $k_x = 1$ component, which is equal to $-\mathscr{E}_{10}$ (being equal and opposite to the energy transfer rate to $k_x = 1$ from the $k_x = 0$ component), and the energy transferred to $k_x = 0$ by the Reynolds stress divergence of the small scales, which contributes to the growth at rate:

$$\mathscr{E}_{0>} = \left(Z^0, R^0\right) + \left(R^0, Z^0\right) \ , \tag{27}$$

with $R^0 \equiv R^0(C - C^e)$. Having removed the energy source sustaining the equilibrium flow, the energy of Z^0 is dissipated at the rate:

$$\mathscr{E}_{0\mathrm{D}} = \left(A_{\mathrm{D}}(Z^0 - Z^e), Z^0\right) + \left(Z^0, A_{\mathrm{D}}(Z^0 - Z^e)\right) \ . \tag{28}$$

The instantaneous rate of change of the energy of the Z^0 and Z^1 components are then $\dot{E}_0 = \mathscr{E}_{01} + \mathscr{E}_{0>} + \mathscr{E}_{0\mathrm{D}}$ and $\dot{E}_1 = \mathscr{E}_{10} + \mathscr{E}_{1>} + \mathscr{E}_{1\mathrm{D}}$. By dividing each term of $\dot{E}_1$ with $2(Z^1, Z^1)$ we obtain, corresponding to (19), (21), (22), the instantaneous growth rates σ_{10}, $\sigma_{1>}$ and $\sigma_{1\mathrm{D}}$ and by dividing $\dot{E}_0$ with $2(Z^0 - Z^e, Z^0 - Z^e)$ the growth rates σ_{01}, $\sigma_{0>}$ and $\sigma_{0\mathrm{D}}$. As equilibration is approached the sum of these growth rates approaches zero, while the evolution of the growth rates indicates the role of each energy transfer rate in producing the equilibration.

Consider first the equilibration of the $n_x = 1$ instability at $\varepsilon/\varepsilon_c = 9$. We impose on the jet equilibrium the most unstable S3T $n_x = 1$ eigenfunction at small amplitude, in order to initiate its exponential growth phase. The evolution of the energy of the Z^1 component of the flow as a function of time, shown in Fig. 6a, confirms the accuracy of our methods for determining the structure and the growth rate of the maximally growing S3T eigenfunction of the jet equilibrium. The contribution of each of the growth rates associated with (24)-(26) to the total normalized energy growth rate of the $k_x = 1$ component of the flow, $\dot{E}_1$, is shown in Fig. 6b. As discussed earlier, the S3T instability is due to the transfer of energy from the zonal flow and the equilibration is seen to be achieved by reducing the transfer of the energy from the mean flow to the $k_x = 1$ component by reducing the tilt of the non-zonal component of the flow. The Reynolds stress contribution remains approximately energetically neutral. The flow eventually equilibrates to a nearly zonal configuration which is very close to the initial jet, as shown in Fig. 7c. The equilibrium state is nearly zonal with an embedded traveling wave (cf. Fig. 7a,b). The wave propagates westward with phase speed indistinguishable from that of the unstable $n_x = 1$ S3T eigenfunction, as can be seen in the Hovmöller diagram of Ψ^1, shown in Fig. 7d. The PV gradient of the equilibrated jet $\beta - \partial_y^2 U^0$ is everywhere positive and the wave propagates in the retrograde part of jet where the PV gradient is close to uniform. Also the structure of the non-zonal component of the equilibrated flow is very close to the structure of the most unstable eigenfunction, as seen by comparing Fig. 4d with Fig. 7b. This equilibrated state is robustly attracting. When the unstable jet is perturbed with random high amplitude perturbations the unstable S3T jet is attracted to the same equilibrium. Mixed S3T equilibria of similar form have been found as statistical equilibria of the full nonlinear equations (Bakas and Ioannou 2013a, 2014).

The equilibration of the jet at $\varepsilon/\varepsilon_c = 13.65$ involves the equilibration of two S3T instabilities, of the powerful $n_x = 0$ jet instability that grows initially at the rate $\sigma_r = 0.32$ and of the weaker $n_x = 1$ instability that grows initially at rate $\sigma_r = 0.08$. We impose on the equilibrium the most unstable S3T $n_x = 0$ and $n_x = 1$ eigenfunctions at small but equal amplitudes, in order to initiate their exponential growth phases. The evolution of the energy of the $Z - Z^e$ component of the flow as a function of time (cf. Fig. 8a) shows initial growth at the rate of the faster $n_x = 0$ instability. The equilibration process for the $n_x = 0$ instability is shown in Fig. 8b, and the equilibration of the $n_x = 1$ instability in Fig. 8c. The $n_x = 0$ instability is supported by the transfer of energy to the $k_x = 0$ component from the small scales ($\sigma_{0>} > 0$) as is the equilibrated jet. The equilibration of this instability proceeds rapidly and is affected by reduction of the $\sigma_{0>}$, i.e. the transfer of energy from the small scales. During the equilibration process there is a pronounced transient enhancement of the transfer rate to the mean flow by the eddies. This leads to the equilibrated jet shown in Fig. 9a,c which has 5% greater energy than the original S3T unstable equilibrium jet. The equilibrated jet is asymmetric with enhanced power at $n_y = 1$. (In this case the unstable $n_y = 2$ jet did not merge with the $n_y = 1$ jet to form a jet with a single jet structure.) During the equilibration process σ_{01} is always negative, indicating continual transfer of mean jet energy supporting the $n_x = 1$ perturbation. The equilibration of the $n_x = 1$ is slower and proceeds in this example, in which the jets did not merge, independently of evolution of the $n_x = 0$ instability. The wave is supported by Reynolds stress divergence from the small scales and from transfer of energy from the mean flow. The former remained unaffected during the equilibration process and equilibration was achieved by reduction of the transfer σ_{10}. The PV gradient of the mean flow, $\beta - \partial_y^2 U^0$, shown in Fig. 9b is positive almost everywhere and the wave is trapped at the prograde part of the jet. As in the case with $\varepsilon/\varepsilon_c = 9$ the wave propagates at the speed of the S3T eigenfunction (cf. Fig. 9d).

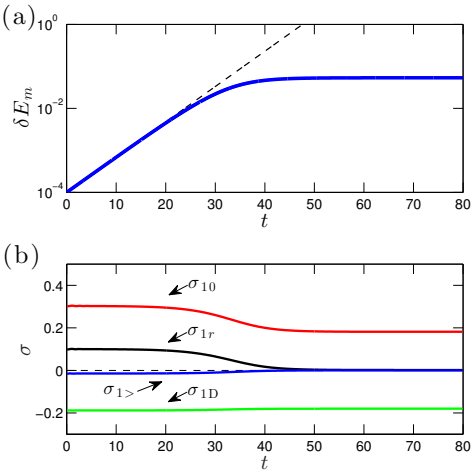

FIG. 6. (a) Evolution of the disturbance energy, δE_m, of the deviation of the large-scale flow $Z - Z^e$, where Z^e is the zonal equilibrium vorticity, at $\varepsilon/\varepsilon_c = 9$. The S3T equilibrium is initially perturbed with the unstable $n_x = 1$ S3T eigenfunction shown in Fig. 4d. Initially the deviation grows at the predicted exponential growth rate of the eigenfunction (dashed) and the equilibration of this instability produces asymptotically the stationary state shown in Fig. 7a,b comprising a jet with a finite amplitude embedded wave. (b) Evolution of the energetics of the $k_x = 1$ component of the flow. Shown are the contribution to the instantaneous growth rate of $k_x = 1$ from energy transferred from the mean flow (σ_{10}), from the small scales ($\sigma_{1>}$) and that lost to dissipation (σ_{1D}). Also shown is the resulting instantaneous growth rate: $\sigma_{1r} = \sigma_{10} + \sigma_{1>} + \sigma_{1D}$, which necessarily vanishes as equilibration is approached. The S3T instability is supported in this case solely from energy transferred to $k_x = 1$ from U^0 and equilibration is achieved by reducing this transfer.

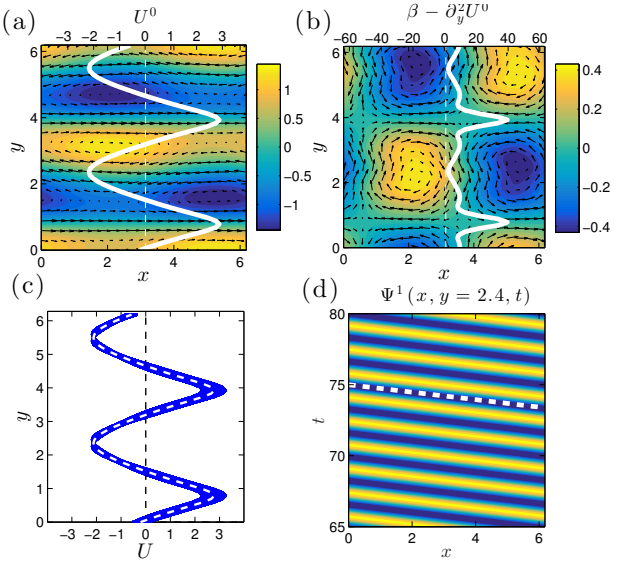

FIG. 7. (a) Snapshot of the instantaneous streamfunction, Ψ, at $t = 80$, and the velocity field of the $k_x = 0$ and $k_x = 1$ components of the equilibrium at $\varepsilon/\varepsilon_c = 9$ resulting from equilibration of the $n_x = 1$ instability. Also shown in white is U^0. The equilibrium consists of a jet and a traveling wave that has no critical layer in the flow as it travels retrograde with respect to the minimum jet velocity. (b) The wave component of the flow, Ψ^1, and its associated velocity field. The wave propagates in the retrograde part of the jet where the potential vorticity gradient, $\beta - \partial_y^2 U^0$ (shown in white) has a small and nearly constant positive value. (c) Variation of the zonal flow velocity, U, with y at equilibrium at different x sections. Also shown is U^0 (dashed line) which is nearly identical to the unstable S3T jet U^e. (d) Hovmöller diagram of Ψ^1 at the location of the minimum of U^0, $y = 2.4$. The phase velocity of the equilibrated wave is equal to the phase speed (indicated with the dashed line) of the most unstable S3T eigenfunction shown in Fig. 4d.

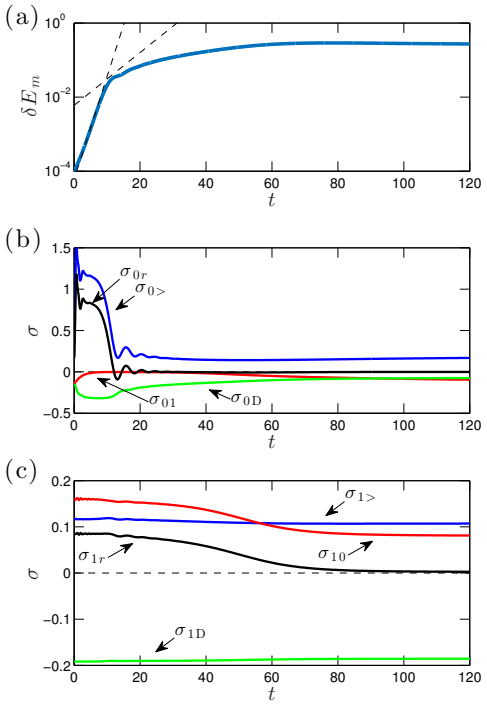

FIG. 8. Evolution of the disturbance energy, δE_m, of the deviation of the large-scale flow $Z - Z^e$, where Z^e is the zonal equilibrium vorticity, at $\varepsilon/\varepsilon_c = 13.65$. The S3T equilibrium is initially perturbed with the unstable $n_x = 0$ and $n_x = 1$ S3T eigenfunctions at small but equal amplitude. The $n_x = 0$ eigenfunction grows at $\sigma_r = 0.32$; the $n_x = 1$ at $\sigma_r = 0.08$ (both indicated with dashed lines). Energy grows at first at the rate of the $n_x = 0$ instability, up to $t \approx 12$, at which time the equilibration of Z^0 is established. The equilibration of Z^1 is not established until $t \approx 60$. (b) Evolution of the energetics of the Z^0. Shown are the contribution to the instantaneous growth rate of $Z^0 - Z^e$ from energy transferred: from Z^1 (σ_{01}), from the small scales ($\sigma_{0>}$), and that lost to dissipation (σ_{0D}). Also shown is the actual instantaneous growth rate, σ_{0r}, which vanishes at equilibration. The $n_x = 0$ S3T instability is supported by the transfer of energy from the small scales and equilibration is achieved rapidly by reducing this transfer. (c) Same as (b) but for Z^1. Shown are the transfer rate from Z^0 (σ_{10}), from the small scales ($\sigma_{1>}$) and the energy dissipation rate σ_{1D}. The $n_x = 1$ instability is supported by both transfer from Z^0 and from small scales and the equilibration is established by reducing the transfer from Z^0.

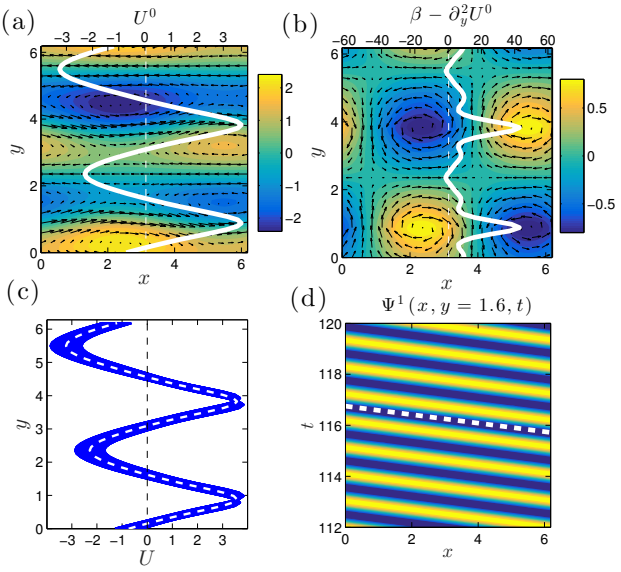

FIG. 9. (a) Snapshot of the instantaneous streamfunction, Ψ, at $t = 120$, and the velocity field of the $k_x = 0$ and $k_x = 1$ components of the equilibrium at $\varepsilon/\varepsilon_c = 13.65$ resulting from equilibration of both the $n_x = 0$ and $n_x = 1$ instabilities. Also shown in white is U^0. The equilibrium consists of a jet and a traveling wave that has no critical layer in the flow as it travels retrograde with respect to all U^0. (b) The wave component of the flow, Ψ^1, and its associated velocity field. The wave is trapped in the prograde part of the flow where the potential vorticity gradient (shown in white) is large. (c) Variation of the zonal flow velocity, U, with y at equilibrium at different x sections. Also shown is U^0 (dashed line) which is nearly identical to the unstable S3T jet U^e. The equilibrated jet is asymmetric. (d) Hovmöller diagram of Ψ^1 at the location of the zero of U^0, $y = 1.6$. The phase velocity of the equilibrated wave is equal to the phase speed (indicated with the dashed line) of the most unstable S3T eigenfunction shown in Fig. 5d.

8. Conclusions

Large-scale structures such as jets, meandering jets and waves embedded in jets are characteristic features of turbulence in planetary atmospheres. While conservation of energy and enstrophy in inviscid 2D turbulence predicts spectral evolution leading to concentration of energy at large scales, these considerations can not predict the phase of the spectral components and therefore can not address the central question of the organization of the energy into specific structural forms such as jets and embedded planetary scale waves in the turbulent jet regime. In order to study structural organization additional aspects of the dynamics beyond conservation principles must be incorporated in the analysis. For this purpose SSD models have been developed and used to study the formation of coherent structure in planetary scale turbulence. In this work an SSD model was formulated for the purpose of studying the regime of coexisting jets and waves. In this model a separation is made by projection onto coherent structure equation in which only the largest zonal harmonics are retained while the remaining spectrum gives rise to the ensemble mean second order statistics associated with the incoherent turbulence. This second order SSD model is closed by a stochastic forcing parameterization that accounts for both the neglected nonlinear dynamics of the small scales as well as the forcing maintaining the turbulence. The equation for the large scales retains its nonlinearity and its interaction through Reynolds stress with the perturbations.

In this model jets form as instabilities and equilibrate at finite amplitude. A stable mode of the Rossby wave spectrum associated with these jets is destabilized for sufficiently strong forcing by interaction with perturbation Reynolds stresses. This destabilization is found to have in some cases the remarkable property of resulting from destabilization of the retrograde Rossby wave to mean jet interaction by structural modification of this damped mode arising from its interaction with the incoherent turbulence thereby transforming it into an unstable mode of the mean jet. In other cases comparable contributions are found from direct forcing by the Reynolds stresses, as in S3T instability with projections at $K = 0$, and induced jet/wave interaction, as in traditional hydrodynamic instability. This synergistic interaction provides a powerful new mechanism for maintaining planetary waves that will be the subject of further investigation.

Acknowledgments. We thank Nikolaos Bakas for useful discussions on the energetics of the equations in spectral space. N.C.C. would like to thank Prof. Georgios Georgiou for his hospitality and support during the summer of 2015 at the University of Cyprus. B.F.F. was supported by NSF AGS-1246929.

References

Bakas, N. A., N. C. Constantinou, and P. J. Ioannou, 2015: S3T stability of the homogeneous state of barotropic beta-plane turbulence. *J. Atmos. Sci.*, **72 (5)**, 1689–1712, doi:10.1175/JAS-D-14-0213.1.

Bakas, N. A., and P. J. Ioannou, 2011: Structural stability theory of two-dimensional fluid flow under stochastic forcing. *J. Fluid Mech.*, **682**, 332–361, doi:10.1017/jfm.2011.228.

Bakas, N. A., and P. J. Ioannou, 2013a: Emergence of large scale structure in barotropic β-plane turbulence. *Phys. Rev. Lett.*, **110**, 224 501, doi:10.1103/PhysRevLett.110.224501.

Bakas, N. A., and P. J. Ioannou, 2013b: On the mechanism underlying the spontaneous emergence of barotropic zonal jets. *J. Atmos. Sci.*, **70 (7)**, 2251–2271, doi:10.1175/JAS-D-12-0102.1.

Bakas, N. A., and P. J. Ioannou, 2014: A theory for the emergence of coherent structures in beta-plane turbulence. *J. Fluid Mech.*, **740**, 312–341, doi:10.1017/jfm.2013.663.

Baldwin, M. P., P. B. Rhines, H.-P. Huang, and M. E. McIntyre, 2007: The jet-stream conundrum. *Science*, **39**, 467–468, doi:10.1126/science.1131375.

Balk, A. M., and T. Yoshikawa, 2009: The Rossby wave extra invariant in the physical space. *Physica D*, **238**, 384–394, doi:10.1016/j.physd.2008.11.008.

Berloff, P., I. Kamenkovich, and J. Pedlosky, 2009: A mechanism of formation of multiple zonal jets in the oceans. *J. Fluid Mech.*, **628**, 395–425, doi:10.1017/S0022112009006375.

Bernstein, J., and B. F. Farrell, 2010: Low frequency variability in a turbulent baroclinic jet: Eddy–mean flow interactions in a two-level model. *J. Atmos. Sci.*, **67 (2)**, 452–467, doi:10.1175/2009JAS3170.1.

Bouchet, F., and A. Venaille, 2012: Statistical mechanics of two-dimensional and geophysical flows. *Phys. Rep.*, **515 (5)**, 227–295, doi:10.1016/j.physrep.2012.02.001.

Connaughton, C. P., B. T. Nadiga, S. V. Nazarenko, and B. E. Quinn, 2010: Modulational instability of Rossby and drift waves and generation of zonal jets. *J. Fluid Mech.*, **645**, 207–231, doi:10.1017/S0022112010000510.

Constantinou, N. C., 2015: Formation of large-scale structures by turbulence in rotating planets. Ph.D. thesis, National and Kapodistrian University of Athens, Athens, URL http://www.didaktorika.gr/eadd/handle/10442/35501?locale=en.

Constantinou, N. C., B. F. Farrell, and P. J. Ioannou, 2014: Emergence and equilibration of jets in beta-plane turbulence: applications of Stochastic Structural Stability Theory. *J. Atmos. Sci.*, **71 (5)**, 1818–1842, doi:10.1175/JAS-D-13-076.1.

Cross, M., and H. Greenside, 2009: *Pattern formation and dynamics in nonequilibrium systems*. Cambridge University Press, 552 pp.

Dritschel, D. G., and M. E. McIntyre, 2008: Multiple jets as PV staircases: The Phillips effect and the resilience of eddy-transport barriers. *J. Atmos. Sci.*, **65**, 855–874, doi:10.1175/2007JAS2227.1.

Farrell, B. F., and P. J. Ioannou, 2002: Perturbation growth and structure in uncertain flows. Part II. *J. Atmos. Sci.*, **59 (18)**, 2647–2664, doi:10.1175/1520-0469(2002)059<2647:PGASIU>2.0.CO;2.

Farrell, B. F., and P. J. Ioannou, 2003: Structural stability of turbulent jets. *J. Atmos. Sci.*, **60**, 2101–2118, doi:10.1175/1520-0469(2003)060<2101:SSOTJ>2.0.CO;2.

Farrell, B. F., and P. J. Ioannou, 2007: Structure and spacing of jets in barotropic turbulence. *J. Atmos. Sci.*, **64**, 3652–3665, doi:10.1175/JAS4016.1.

Farrell, B. F., and P. J. Ioannou, 2008: Formation of jets by baroclinic turbulence. *J. Atmos. Sci.*, **65**, 3353–3375, doi:10.1175/2008JAS2611.1.

Farrell, B. F., and P. J. Ioannou, 2009a: Emergence of jets from turbulence in the shallow-water equations on an equatorial beta plane. *J. Atmos. Sci.*, **66**, 3197–3207, doi:10.1175/2009JAS2941.1.

Farrell, B. F., and P. J. Ioannou, 2009b: A theory of baroclinic turbulence. *J. Atmos. Sci.*, **66**, 2444–2454, doi:10.1175/2009JAS2989.1.

Farrell, B. F., and P. J. Ioannou, 2015: Statistical State Dynamics: a new perspective on turbulence in shear flow. *Zonal jets*, B. Galperin, and P. L. Read, Eds., Cambridge University Press, chap. 5, (submitted, arXiv:1412.8290).

Fjørtoft, R., 1953: On the changes in the spectral distribution of kinetic evergy for twodimensional, nondivergent flow. *Tellus*, **5**, 120–140, doi:10.1111/j.2153-3490.1953.tb01051.x.

Frisch, U., 1995: *Turbulence: The Legacy of A. N. Kolmogorov*. Cambridge University Press.

Gill, A. E., 1974: The stability of planetary waves on an infinite beta-plane. *Geophys. Astrophys. Fluid Dyn.*, **6**, 29–47, doi:10.1080/03091927409365786.

Huang, H.-P., and W. A. Robinson, 1998: Two-dimensional turbulence and persistent zonal jets in a global barotropic model. *J. Atmos. Sci.*, **55**, 611–632, doi:10.1175/1520-0469(1998)055<0611:TDTAPZ>2.0.CO;2.

Kasahara, A., 1980: Effect of zonal flows on the free oscillations of a barotropic atmosphere. *J. Atmos. Sci.*, **37**, 917–929, doi:10.1175/1520-0469(1980)037<0917:EOZFOT>2.0.CO;2.

Lorenz, E. N., 1972: Barotropic instability of Rossby wave motion. *J. Atmos. Sci.*, **29**, 258–269, doi:10.1175/1520-0469(1972)029<0258:BIORWM>2.0.CO;2.

Manfroi, A. J., and W. R. Young, 1999: Slow evolution of zonal jets on the beta plane. *J. Atmos. Sci.*, **56**, 784–800, doi:10.1175/1520-0469(1999)056<0784:SEOZJO>2.0.CO;2.

Marston, J. B., E. Conover, and T. Schneider, 2008: Statistics of an unstable barotropic jet from a cumulant expansion. *J. Atmos. Sci.*, **65 (6)**, 1955–1966, doi:10.1175/2007JAS2510.1.

Miller, J., 1990: Statistical mechanics of Euler equations in two dimensions. *Phys. Rev. Lett.*, **65**, 2137–2140, doi:10.1103/PhysRevLett.65.2137.

Parker, J. B., 2014: Zonal flows and turbulence in fluids and plasmas. Ph.D. thesis, Princeton, URL http://arks.princeton.edu/ark:/88435/dsp01h989r543m.

Parker, J. B., and J. A. Krommes, 2013: Zonal flow as pattern formation. *Phys. Plasmas*, **20**, 100 703, doi:10.1063/1.4828717.

Parker, J. B., and J. A. Krommes, 2014: Generation of zonal flows through symmetry breaking of statistical homogeneity. *New J. Phys.*, **16 (3)**, 035 006, doi:10.1088/1367-2630/16/3/035006.

Rhines, P. B., 1975: Waves and turbulence on a beta-plane. *J. Fluid Mech.*, **69**, 417–433, doi:10.1017/S0022112075001504.

Robert, R., and J. Sommeria, 1991: Statistical equilibrium states for two-dimensional flows. *J. Fluid Mech.*, **229**, 291–310, doi:10.1017/S0022112091003038.

Sánchez-Lavega, A., and Coauthors, 2014: The long-term steady motion of Saturn's hexagon and the stability of its enclosed jet stream under seasonal changes. *Geophys. Res. Lett.*, **41 (5)**, 1425–1431, doi:10.1002/2013GL059078, 2013GL059078.

Scott, R. K., and D. G. Dritschel, 2012: The structure of zonal jets in geostrophic turbulence. *J. Fluid Mech.*, **711**, 576–598, doi:10.1017/jfm.2012.410.

Shepherd, T. G., 1987: A spectral view of nonlinear fluxes and stationary transient interaction in the atmosphere. *J. Atmos. Sci.*, **44**, 1166–1178, doi:10.1175/1520-0469(1987)044<1166:ASVONF>2.0.CO;2.

Srinivasan, K., and W. R. Young, 2012: Zonostrophic instability. *J. Atmos. Sci.*, **69 (5)**, 1633–1656, doi:10.1175/JAS-D-11-0200.1.

Tobias, S. M., and J. B. Marston, 2013: Direct statistical simulation of out-of-equilibrium jets. *Phys. Rev. Lett.*, **110 (10)**, 104 502, doi:10.1103/PhysRevLett.110.104502.

Vasavada, A. R., and A. P. Showman, 2005: Jovian atmospheric dynamics: an update after *Galileo* and *Cassini*. *Rep. Prog. Phys.*, **68**, 1935–1996, doi:10.1088/0034-4885/68/8/R06.

Wordsworth, R. D., 2009: A phase-space study of jet formation in planetary-scale fluids. *Phys. Fluids*, **21**, 056 602, doi:10.1063/1.2990042.

Wordsworth, R. D., P. L. Read, and Y. H. Yamazaki, 2008: Turbulence, waves, and jets in a differentially heated rotating annulus experiment. *Phys. Fluids*, **20**, 126 602, doi:10.1063/1.2990042.